Dysfunctional Connections Between the Nucleus and the Actin and Microtubule Networks in Laminopathic Models

Christopher M. Hale,* Arun L. Shrestha,* Shyam B. Khatau,* P. J. Stewart-Hutchinson,† Lidia Hernandez,‡ Colin L. Stewart,§ Didier Hodzic,† and Denis Wirtz*¶

*Department of Chemical and Biomolecular Engineering, †Department of Cell Biology and Physiology, Washington University School of Medicine, St. Louis, Missouri; ‡Cancer and Developmental Biology, National Cancer Institute, Frederick, Maryland; §Institute of Medical Biology, Immunos, Singapore; and ¶Howard Hughes Medical Institute Graduate Training Program (NBMed) and Institute for NanoBioTechnology, Johns Hopkins University, Baltimore, Maryland

ABSTRACT Laminopathies encompass a wide array of human diseases associated to scattered mutations along LMNA, a single gene encoding A-type lamins. How such genetic alterations translate to cellular defects and generate such diverse disease phenotypes remains enigmatic. Recent work has identified nuclear envelope proteins—emerin and the linker of the nucleoskeleton and cytoskeleton (LINC) complex—which connect the nuclear lamina to the cytoskeleton. Here we quantitatively examine the composition of the nuclear envelope, as well as the architecture and functions of the cytoskeleton in cells derived from two laminopathic mouse models, including Hutchinson-Gilford progeria syndrome ($Lmna^{L530P/L530P}$) and Emery-Dreifuss muscular dystrophy ($Lmna^{-/-}$). Cells derived from the overtly aphenotypical model of X-linked Emery-Dreifuss muscular dystrophy ($Emd^{-/y}$) were also included. We find that the centrosome is detached from the nucleus, preventing centrosome polarization in cells under flow—defects that are mediated by the loss of emerin from the nuclear envelope. Moreover, while basal actin and focal adhesion structure are mildly affected, RhoA activation, cell-substratum adhesion, and cytoplasmic elasticity are greatly lowered, exclusively in laminopathic models in which the LINC complex is disrupted. These results indicate a new function for emerin in cell polarization and suggest that laminopathies are not directly associated with cells' inability to polarize, but rather with cytoplasmic softening and weakened adhesion mediated by the disruption of the LINC complex across the nuclear envelope.

INTRODUCTION

Laminopathies are a family of diseases caused by mutations in the genes responsible for the proteins that make up the nuclear lamina. Over 200 missense mutations in the gene-encoding lamins A and C (*LMNA*) are associated with at least 13 known diseases (1), such as Hutchinson-Gilford progeria syndrome (HGPS) (2), atypical Werner syndrome (3), Emery-Dreifuss muscular dystrophy (EDMD) (4), and dilated cardiomyopathy (5), among others. Though laminopathies are related by the gene in which their mutations originate, a broad range of symptoms exists across the diseases. Defects include premature ageing, atherosclerosis, cardiomyopathy, muscular dystrophy, lipodystrophy, scleroderma, growth retardation, and in some cases, a combination of these pathologies. In the process of studying these diseases and the cellular mechanisms in which they manifest, the multiple functions of the nuclear lamina are also being revealed (6). Formerly thought to function mainly as a nuclear scaffold, the nuclear lamina has been found to interact with several proteins and play important roles in chromatin organization, gene regulation, and signal transduction (7,8), and potentially have downstream effects on cell polarization, adhesion, and mechanics via cytoskeletal linker proteins (9). Thus, two nonexclusive schools of thought seek to explain the mechanism behind laminopathic disease: the structural hypothesis suggests that nuclear and perhaps cellular fragility have pathologic consequences in mechanically strained tissues, while the gene-regulation hypothesis attributes tissue-specific defects to impaired binding of lamin and transcriptional regulators.

The nuclear lamina is a 10–20 nm-thick protein meshwork consisting of primarily A- and B-type lamins (10) that lines the nucleoplasmic side of the inner nuclear membrane. Lamins are type V intermediate filaments, which are composed of a coiled-coil domain belted by an N-terminal head domain and a C-terminal tail domain; unlike other intermediate filaments, lamins also contain a nuclear localization signal. While B-type lamins are essential for viability (11) and remain membrane-bound during mitosis (12), the expression of A-type lamins is developmentally regulated (13) and tissue-specific (14), and they disperse as soluble proteins during mitosis (7). Lamins bind to a wide array of partners within the nucleus, including transcription factors, nuclear pore complexes, and several inner nuclear membrane proteins including emerin (15); Sun proteins (16,17); Nesprin isoforms (18,19); lamina-associated proteins 1 and 2, i.e., LAP1 and LAP2 (20,21); the lamin B receptor, i.e., LBR; and MAN1 (1,18,19). Of particular interest in this study is the involvement of A-type lamins in anchoring multiprotein complexes that form a bridge between the inner nuclear membrane and the cellular cytoskeleton (10).

Submitted June 5, 2008, and accepted for publication August 25, 2008.

Address reprint requests to Denis Wirtz, Tel.: 410-516-7006; E-mail: wirtz@jhu.edu; or to Didier Hodzic, E-mail: dhodzic@wustl.edu.

Editor: Edward H. Egelman.

0006-3495/08/12/5462/14 $2.00

doi: 10.1529/biophysj.108.139428

At the cellular level, the laminopathic phenotype is characterized by abnormalities in nuclear shape, as well as cellular fragility (22,23) and a decreased cytoplasmic elasticity, as we and others demonstrated previously in *Lmna*$^{-/-}$ mouse embryonic fibroblasts (9,23). Here we hypothesize that laminopathic defects could stem from dysfunctional connections between the nucleus and cytoskeleton, which would subsequently disrupt cellular functions mediated by the cytoskeleton. We probe the localization of lamin-binding proteins and their partners and examine the biophysical properties of cells derived from three different mouse models: knock-in mice in which the *Lmna* gene has been replaced with a mutant *Lmna* gene (*Lmna*$^{L530P/L530P}$) and mice lacking either lamin A/C (*Lmna*$^{-/-}$) or emerin (*Emd*$^{-/y}$). *Lmna*$^{L530P/L530P}$ mice display phenotypes similar to human Hutchinson-Gilford progeria syndrome (HGPS) (24), while *Lmna*$^{-/-}$ mice display phenotypes reminiscent of autosomal-dominant Emery-Dreifuss muscular dystrophy (AD-EDMD) (25,26). *Emd*$^{-/y}$ mice do not show any overt pathological phenotype (27), although defects in muscle regeneration pathways have been found (28). Thus, although possibly a genetic model for the nuclear envelopathy of X-linked EDMD (XL-EDMD), mice do not fully recapitulate EDMD. Using cells from progeric and muscular dystrophy mouse models, we show that a disorganized lamin network disrupts emerin localization, causing an increase in the distance between the nucleus and the microtubule organizing center (MTOC), as well as causing the failure of these cells to polarize in response to a shear flow stimulus. Increased MTOC-nucleus distancing and abrogated polarization was also observed in emerin-null cells. Previous work also supports the existence of a nucleus connection with the actin cytoskeleton via Sun and Nesprin proteins, which collectively form the linker of nucleus and cytoskeleton, or linker of the nucleoskeleton and cytoskeleton (LINC complex) (16). Here we show that LINC complexes are defective exclusively in laminopathic models, and that as a result, actin-mediated cellular functions—including cell adhesion, cell migration, and cell mechanics—are adversely affected. Though the laminopathic and emerin-null models demonstrate an inability to position their MTOC and polarize their microtubule network, our results suggest a preferential correlation between laminopathic phenotypes and defective actin-mediated cellular functions.

MATERIALS AND METHODS

Cell culture

Derivation and culture of wild-type and *Lmna*$^{L530P/L530P}$ mouse adult fibroblasts (MAFs), *Lmna*$^{+/+}$ and *Lmna*$^{-/-}$ mouse embryonic fibroblasts (MEFs), and *Emd*$^{+/y}$ and *Emd*$^{-/y}$ MEFs have been previously characterized (9,24,27). MAFs were cultured in DMEM (ATCC, Manassas, VA) supplemented with 10% bovine calf serum (BCS, ATCC) and 100 U penicillin and 100 μg streptomycin (Sigma, St. Louis, MO) and maintained at 37°C in a humidified, 5% CO_2 environment. MEFs were cultured under similar conditions, but with fetal bovine serum (ATCC) instead of BCS. MAFs were passaged every 3–4 days for a maximum of three passages, after which doubling capacity decreases (24); similarly, MEFs (initial passage (23)) were passaged every 2–3 days for a maximum of six passages. For immunofluorescence microscopy, cells were seeded at $\sim 2 \times 10^3$ cells/ml on 35-mm glass bottom dishes precoated with collagen (MatTek, Ashland, MA). For shear-induced polarization experiments, 75-mm glass microscope slides (Fisher Scientific, Pittsburg, PA) were cleaned in ethanol, rinsed, and coated with collagen type I from rat tail (BD Biosciences, San Jose, CA) at 50 μg/ml concentration for 1 h; after rinsing, cells were then seeded at $\sim 2 \times 10^3$ cells/ml. For wound-healing experiments, 24-well glass bottom dishes (MatTek) were coated with collagen (as described above) and seeded with cells at $\sim 1 \times 10^4$ cells/ml. For ballistic nanoparticle injection, cells were seeded at $\sim 1 \times 10^4$ cells/ml on 10-cm cell culture dishes (Corning, Corning, NY). After bombardment and recovery, cells were then seeded at $\sim 2 \times 10^3$ cells/ml on 35-mm glass bottom collagen-coated dishes.

Immunofluorescence microscopy

Cells plated on glass bottom collagen-coated dishes were fixed with 3.7% formaldehyde for 30 min, washed with 1× phosphate-buffered saline (PBS) at room temperature (RT) and permeabilized with 0.1% Triton X-100 for 10 min. PBS supplemented with BCS (10%) was used to block nonspecific binding, after which cells were treated with primary and secondary antibodies, respectively, at proper dilutions for 1 h each at RT. For lamin A staining, cells were incubated with a monoclonal mouse anti-lamin A antibody (Abcam, Cambridge, MA) at 1:200 dilution, and subsequently incubated in Alexa Fluor 568 goat anti-mouse antibody (Invitrogen, Carlsbad, CA) at 1:200 dilution. For supplemental stains, anti-lamin A/C (131C3) monoclonal antibody (Chemicon, Billerica, MA) was used at 1:100 dilution. Monoclonal emerin antibody (Novocastra, Clone 4G5) and Sun1 antibody were kindly provided by Dr. Shackleton (29). The generation of antibodies from rabbit Sun2 and Nesprin3 antisera, kindly provided by Dr. A. Sonnenberg (The Netherlands Cancer Institute), have been described (30,31). Rabbit anti-Nesprin2giant antibody, kindly provided by Drs. E. Gomes and G. Gundersen (Columbia University), was raised against the actin-binding domain of Nesprin2 giant. For staining of the above proteins, cells were incubated with either anti-emerin, anti-Sun1, anti-Sun2, anti-Nesprin2 giant, or anti-Nesprin3 at 1:200, 1:1000, 1:2000, 1:500, or 1:1000 dilution, respectively, followed by incubation with Alexa Fluor 488 or 594 goat anti-rabbit antibody (Invitrogen) at 1:200 dilution. Nuclear DNA was stained during secondary treatment using 300 nM DAPI. Cells were then cured in ProLong Gold antifade reagent (Sigma) and then covered with a coverslip before visualization. Fluorescent micrographs, unless otherwise noted, were collected using a Cascade 1 K CCD camera (Roper Scientific, Tucson, AZ) mounted on a Nikon TE2000E microscope with a 60× Plan Fluor lens (NA 1.4, Nikon, Melville, NY) controlled by Metavue (Universal Imaging, West Chester, PA). Images were digitally overlaid using Metamorph (Universal Imaging). Images of emerin, Sun1, Sun2, Nesprin2 giant, and Nesprin3 staining (Fig. 1, rows 2–6) were collected with a 63× oil immersion objective (1.4 NA, Plan-Achromat, Zeiss, Peabody, MA) on an Axioplan microscope (Zeiss) outfitted with a confocal laser scanning head (MRC 1024, BioRad, Richmond, CA). The Lasersharp 2000 software package (BioRad) was used to pilot the microscope and format the raw images into .tif files. The latter were further digitally merged using Photoshop (Adobe, San Jose, CA). For each condition, cells were qualitatively assessed as to whether a majority of cells showed intact staining, or a loss of staining, of particular proteins with respect to wild-type localization and intensity.

MTOC-nucleus distance

Cells were plated on collagen, then fixed and stained using a polyclonal rabbit anti-γ-tubulin antibody (Abcam) at 1:500 dilution and subsequently incubated in Alexa Fluor 488 goat anti-rabbit antibody (Invitrogen) at 1:200 dilution. Nuclear DNA was stained with 300 nM DAPI, as described above.

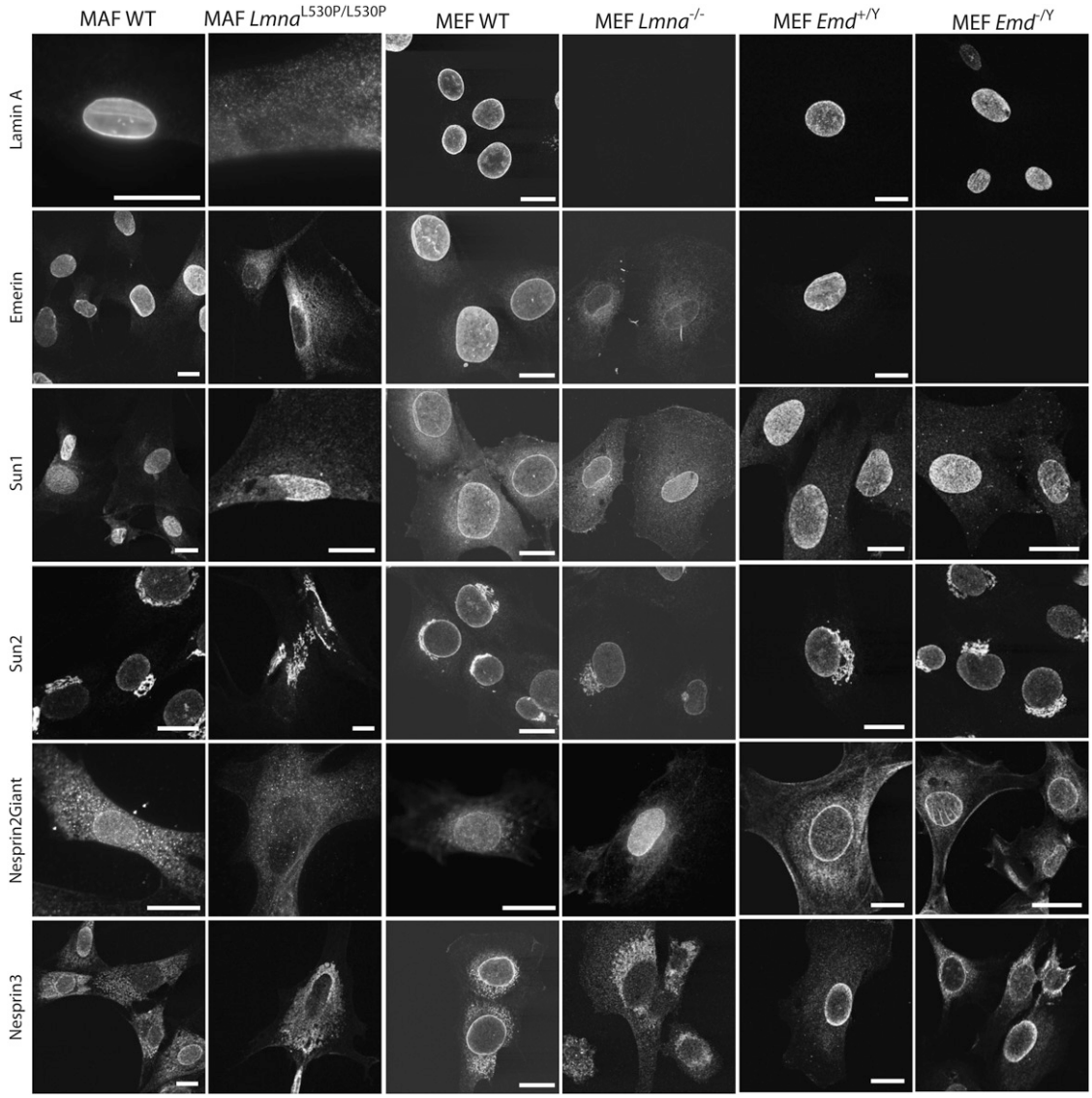

FIGURE 1 Immunolocalization of lamin A and LINC complex components in wild-type and laminopathic fibroblasts. Localization of nuclear lamina protein lamin A, nuclear envelope protein emerin, and LINC complex components Sun1, Sun2, Nesprin2-giant, and Nesprin 3 in wild-type and *Lmna*$^{L530P/L530P}$ (MAFs), *Lmna*$^{+/+}$, *Lmna*$^{-/-}$, *Emd*$^{+/y}$, and *Emd*$^{-/y}$ (MEF) cells. Note that Golgi is stained in Sun2 photos due to antibody cross-reaction; Sun2 localizes only to the inner nuclear membrane. Scale bar, 20 μm; pairs of images are at same scale, unless otherwise indicated.

The distance between the MTOC and the nucleus was determined by overlaying acquired images and extending a line from the centroid of the MTOC to the nearest point of the nuclear rim; the length of this line was measured using Metamorph (Universal Imaging).

Cell polarization

To assess the ability of cells to polarize, cells were plated on collagen and subjected to a flow-based polarization assay. Cells were placed in a parallel-plate flow chamber (GlycoTech, Gaithersburg, MD) using a 0.127-mm-thick gasket with a flow width of 2.5 mm. Cells were subjected to a wall shear stress of 20 dyn/cm^2 for 40 min using a flow of medium buffered with 25 mM HEPES. This shear stress was found to provide an adequate shear stimulus and did not induce significant cell detachment. Post-shear, cells were immediately fixed and stained using a monoclonal mouse anti-α-tubulin antibody (Abcam) at 1:1000 dilution and subsequently incubated in Alexa Fluor 568 goat anti-mouse antibody (Invitrogen) at 1:200 dilution, while nuclear DNA was stained with 300 nM DAPI, as described above. Though cells could have been stained using the γ-tubulin antibody previously mentioned for the sake of locating the MTOC, α-tubulin staining allowed for visualization of both the MTOC and microtubule network. Cells were scored based on the position of the MTOC relative to the nucleus (32). Acquired images were overlaid and the nucleus was divided vertically into two regions. Cells in which the MTOC was located on the side of the nucleus opposing the direction of flow were scored as unpolarized, while cells in which the MTOC was located on the side of the nucleus in the direction of flow were scored as polarized.

Morphometry of focal adhesions

To assess the morphology of focal adhesions, cells were plated on collagen, then fixed and stained using a monoclonal mouse anti-vinculin antibody (Sigma) at 1:40 dilution and subsequently incubated in Alexa Fluor 488 goat anti-mouse antibody (Invitrogen) at 1:200 dilution, as described above. Actin

and nuclear DNA were stained using Alexa Fluor 568 phalloidin (Invitrogen) at 1:40 dilution and DAPI, respectively, during the secondary step. The individual focal-adhesion peripheries were hand-traced, holding camera settings constant across all images acquired and analyzed. Focal adhesion area, shape factor, and length were determined using the integrated morphometry analysis tool of Metamorph (Universal Imaging).

Cell migration

Cell migration assays were conducted, as described previously (9). Briefly, cells were plated on collagen in 24-well collagen coated glass bottom microtiter plates, cultured to confluency, and then simultaneously scratched using a 24-floating pin replicator (V&P Scientific, San Diego, CA). Phase contrast images were collected every hour for 6 h using a 10× Plan Fluor lens (NA 0.3), as described above. During wound healing, cells were kept in a 37°C, 5% CO_2, humidified environment using a live cell chamber (Pathology Devices, Westminster, MD). The rates of cell migration were computed by tracing the edges of the wounds and measuring the changes in wound area not covered by cells between final and initial time points using Metamorph (Universal Imaging). Only wounds whose initial width was within 50 μm of the average initial wound width (490 μm) were analyzed to avoid variability of closure time.

Cell adhesion

Ninety-six-well glass bottom microtiter plates (MatTek) were incubated with 200 ng collagen in 0.02 N acetic acid per well for 2 h at RT. Wells were then rinsed and incubated with 2% BSA, diluted in PBS with 5% 1 M HEPES buffer solution (Invitrogen) for 1 h to block nonspecific binding. Test cells suspended in RPMI media (Invitrogen) were then incubated with 5 μM CalceinAM (Invitrogen) for 30 min at 37°C. CalceinAM is retained in cells with intact membranes; dead cells are not labeled, and the fluorophore is rapidly lost under conditions causing cell lysis. CalceinAM was then removed by centrifugation and repeated washes with 5% HEPES in PBS; cell concentration was then adjusted to 2×10^6 cells/ml. One-hundred microliters of CalceinAM-loaded cells were then added to each well and incubated for 20 min at RT to allow for cell adhesion to the collagen-coated surface. Fluorescence was measured using a microtiter plate reader (Gemini XPS, Molecular Devices), with an excitation wavelength of 485 nm and emission wavelength of 530 nm. The 96-well plate was then placed in a static cell adhesion chamber (Glycotech, Rockville, MD), 5% HEPES in PBS was added, and the chamber was inverted for 6 min to allow cells to detach in a purely liquid environment, void of a liquid-gas interface. The wash chamber was then stood on its end and the plate was gently removed. Percentage adherence was calculated by dividing fluorescence units after wash by fluorescence units before wash.

Extent of F-actin bundling

Whole cell lysates were prepared with protease inhibitors and lysis buffer (Cytoskeleton, Denver, CO) from cultures of $\sim 2 \times 10^7$ cells grown on 10 cm tissue culture dishes. Lysates were centrifuged at 13,000 rpm at 4°C for 10 min. After the supernatant was discarded, pellets were washed with ice-cold PBS and centrifuged again. Pellets were then boiled at 65°C for 5 min in 100 μl of Laemmli buffer. Samples were resolved by 10% SDS-PAGE and transferred to nitrocellulose membranes (0.2 μm pore size, Invitrogen) in semi-dry transfer buffer (25 mM Tris-HCl, pH 8.3, 0.19 M glycine, 20% methanol (analytical grade)) for 90 min at 110 V. Membranes were incubated in blocking buffer (5% powdered milk (w/v) in 1× PBS-Tween (137 mM NaCl, 2.7 mM KCl, 10 mM Na2HPO4, 2 mM KH2PO4, 0.05% Tween-20)) for 1 h at RT. Membranes were then probed with mouse monoclonal anti-actin HRP conjugate (Santa Cruz Biotechnology, Santa Cruz, CA) diluted 1:1000 in blocking buffer for 1 h at RT. After washing the membrane for 20 min with PBS-Tween, blots were developed using ECL (Pierce Biotechnologies, Rockford, IL) and exposed to film (BioMax XAR, Kodak, Rochester, NY) for a period of time.

Western blot for lamin A/C detection

Proteins were separated by SDS-PAGE and transferred to nitrocellulose membrane. Membranes were blocked in 1× Tris-buffered saline with Tween-20 (TBST), 5% milk for 1 h at RT. Primary antibodies were blotted in 1× TBST, 5% milk either for 1 h at RT or overnight at 4°C. Secondary antibody-HRP conjugates were blotted in 1× TBST, 5% milk for 1 h at RT and membranes were stained with SuperSignal West Pico Chemiluminescent Substrate (Pierce Biotechnologies).

L530P sequencing construct

A fragment of *Lmna* (from exon 8 to exon 10) was amplified by PCR from genomic DNA of primary $Lmna^{L530P/L530P}$ mouse fibroblasts extracted with Trizol (Invitrogen). The cDNA was then cloned into pCR2.1 (Invitrogen) by TOPO/TA ligation and sequenced.

Rac and RhoA activation

Rac-GTP and RhoA-GTP were quantified using the G-LISA Rac activation assay and the G-LISA RhoA activation assay Biochem Kits according to the manufacturer's protocol (Cytoskeleton). Lysates were prepared from cultures grown on 10 cm tissue culture dishes at ~70% confluency. All activities were normalized to their respective activities in wild-type littermates.

Cell microrheology

The micromechanical properties of the cytoplasm were measured using ballistic intracellular nanorheology, as described previously (33–35). Briefly, 100 nm-diameter fluorescent polystyrene nanoparticles (Invitrogen) were ballistically injected in the cytoplasm of cells using a Biolistic PDS-1000/HE particle delivery system (BioRad). Cells were repeatedly washed to eliminate endocytosis of the nanoparticles, thus avoiding the possibility of convective, vesicular transport of the particles within the cell. Cells were given several hours to recover post-bombardment, before embedded nanoparticles were tracked with high spatial and temporal resolutions using high-magnification fluorescence microscopy (60×) and multiple-particle tracking software (36). In this study, we did not distinguish between nanoparticles in different regions of the cell. After injection and incubation overnight, nanoparticles dispersed uniformly throughout the entire cytoplasm in both normal and mutant cells for all conditions. Since neither the perinuclear nor lamellar region is overrepresented in each nanoparticle population, the differences detected represent global changes in cytoskeletal stiffness as opposed to location-specific cytoskeletal changes. The mean-squared displacements (MSDs) of individual nanoparticles are calculated from 20 s-long streams of the time-dependent coordinates of the center of each nanoparticle. The mean elasticity of the cytoplasm is calculated from the ensemble-averaged MSD, as described (36). Briefly, the ensemble-averaged MSD of the nanoparticles is related to the complex viscoelastic modulus using the after equation (33),

$$G^*(\omega) = \frac{k_B T}{\pi a i \omega \Im_u\{\langle \Delta r^2(\tau)\rangle\}},$$

where k_B is Boltzmann's constant, T is the absolute temperature of the cell (in Kelvin), a is the radius of the nanoparticles, $\omega = 1/\tau$, τ is the time lag, and $\Im_u\{\langle \Delta r^2(\tau)\rangle\}$ is the Fourier transform of $\langle \Delta r^2(\tau)\rangle$, the time-lag dependent, ensemble-averaged MSD. The above equation can be solved analytically (37), allowing the frequency-dependent elastic modulus to be calculated algebraically using the relationship

$$G'(\omega) = |G^*(\omega)|\cos\left(\frac{\pi a(\omega)}{2}\right),$$

where

$$|G^*(\omega)| = \frac{2k_BT}{3\pi a\langle\Delta r^2(1/\omega)\rangle\Gamma(1+a(\omega))},$$

where α is the local logarithmic slope of $\langle\Delta r^2(\tau)\rangle$ at the frequency of interest and Γ is the γ-function. Here we report the plateau elastic modulus for all conditions.

Nuclear morphology in cells at rest and under shear

Cells were plated on collagen, then fixed and stained for nuclear DNA, as described above. DAPI-stained nuclei were individually traced by hand, holding camera settings constant across all images acquired and analyzed. The shape factor was measured using Metamorph (Universal Imaging) and is equal to $4\pi A/P^2$, where A is the apparent surface area of the shape and P its perimeter; it is unity for a perfect circle and zero for a line segment. Nuclei with poor staining (e.g., *right panels* in Fig. S2 *A* in Supplementary Material, Data S1) complicated the process of tracing, since the nucleus perimeter could not be readily determined; for these cells, the nucleus outline was approximated by accentuating the contrast of images. To circumvent this issue altogether, cell nuclei were also scored as either intact or not intact. A fully stained, ovoid nucleus was scored as intact, receiving a value of 1, while a lobulated nucleus with incomplete staining was scored as not intact, receiving a value of 0 (see Fig. S2 *E* in Data S1 for illustrative images of intact and deformed nuclei). This assessment, though less quantitative, proved more robust by allowing for all nuclei studied to be analyzed by the same assay; a strong correlation between the assessment of nuclear morphology and the shape factor was also observed (see Fig. S2 in Data S1). Nuclear morphology was assessed in cells at rest and in cells subjected to shear stress. Cells were sheared as previously described and immediately fixed after application of shear.

Statistics

Immunofluorescence microscopy, MTOC-nucleus distance, cell polarization (at rest and at shear), focal adhesion analysis, cell migration, cell adhesion, RhoA/Rac activity, ballistic intracellular nanorheology, and nucleus shape factor (in cells at rest and under shear) were assessed in at least three independent experiments for all cell conditions studied. Statistical analysis was performed and mean values and standard error of measurement were calculated and plotted using Graphpad Prism (Graphpad Software, San Diego, CA). Two-tailed unpaired *t*-tests were conducted to determine significance of functional (i.e., cell adhesion, migration, polarization, mechanics, etc.) and ultrastructural differences (i.e., focal adhesion morphology) caused by disease-causing mutations or protein depletion. Significance was indicated using the standard Michelin Guide scale (*** for $p < 0.001$, ** for $p < 0.01$, and * for $p < 0.05$).

RESULTS

Displacement of nuclear envelope proteins in laminopathic cells

Immunofluorescence microscopy was used to qualitatively assess the localization of nuclear envelope-associated proteins that are known to establish nucleo-cytoskeletal connections. These include lamin A, emerin, and LINC complex proteins Sun1, Sun2, Nesprin2 giant, and Nesprin3. *Lmna*$^{L530P/L530P}$ cells displayed loss of emerin, Sun1, Sun2, Nesprin2 giant, and Nesprin 3 signals and a marked reduction of lamin A at the nuclear envelope (NE) compared to their wild-type littermates, in which localization at the NE was evident (*first* and *second columns*, Fig. 1; see also Table 1). Although the presence of the L530P mutation was directly confirmed through the sequencing of a PCR fragment amplified from genomic DNA (see Fig. S1 in Data S1), we were unable to detect lamin A protein in *Lmna*$^{L530P/L530P}$ fibroblasts using different antibodies and types of microscopy. Nevertheless, *Lmna*$^{L530P/L530P}$ fibroblasts express low levels of mutated lamins, perhaps due to a destabilizing effect of the mutation on the protein (23), suggesting that it is these low levels that distinguish the *Lmna*$^{L530P/L530P}$ mouse phenotype from the *Lmna*$^{-/-}$ mouse, in which no lamins or transcripts are present. *Lmna*$^{-/-}$ cells also showed a complete loss of lamin A (as expected), emerin, and Nesprin3 from the nuclear envelope, but increased staining of Nesprin 2 giant, while Sun1 and Sun2 were unaffected (*third* and *fourth columns*, Fig. 1). *Emd*$^{-/y}$ cells, as expected, showed a loss of emerin, while the localization of all other proteins probed remained intact (*fifth* and *sixth columns*, Fig. 1). These results indicate that the absence of lamin A and the disease-causing mutation L530P lead to a significant mislocalization of emerin and proteins involved in the formation of the LINC complexes, while emerin loss alone does not alter the localization of the LINC complex components in the NE (Table 2; and see Fig. 7).

Disruption of the MTOC-nucleus connection and defective MTOC polarization in cells displaying loss of emerin from the NE

It has been suggested that lamin A/C and emerin play a role in linking the nucleus to the microtubule cytoskeleton, and in fact, recent work has shown that lamin A/C (9) or emerin depletion (38) uncouples the MTOC (or centrosome) from the nucleus (Fig. 2). Salpingidou et al. (37) have shown that emerin also localizes to the outer nuclear membrane and have suggested an emerin-microtubule interaction to tether the MTOC to the nucleus based on emerin and β-tubulin binding in vitro (see Fig. 7). Thus, we hypothesized that the emerin displacement observed in the three fibroblast lines studied here would be associated with microtubule defects, particularly an increased MTOC-nucleus distance. Using immuno fluorescence microscopy, we observed no gross changes in microtubule architecture between wild-type and laminopathic cells (data not shown). However, in *Lmna*$^{L530P/L530P}$, *Lmna*$^{-/-}$, and *Emd*$^{-/y}$ cells, in which emerin is lost from the NE, a significant increase in the distance between the MTOC and the nucleus was observed (Fig. 2 *B*). The average distance between MTOC and nucleus was increased approximately sevenfold in *Lmna*$^{L530P/L530P}$ cells compared to their wild-type cells ($P < 0.01$) and to nearly the same extent as in *Lmna*$^{-/-}$ cells (Fig. 2 *B*).

TABLE 1 Summary of results from immunofluorescence microscopy studies

	Localization of nuclear envelope proteins relative to corresponding wild-type			
	WT localization	MAF $Lmna^{L530P/L530P}$	MEF $Lmna^{-/-}$	MEF $Emd^{-/y}$
Lamin A	Near inner nuclear membrane (54)	−*	−	+
Emerin	Inner and outer nuclear membrane (37,55)	−	−	−
Sun1	Inner nuclear membrane (29)	−	+	+
Sun2	Inner nuclear membrane (30)	−	+	+
Nesprin2g	Outer nuclear membrane (56)	−	++	+
Nesprin3	Outer nuclear membrane (31)	−	−	+

Symbols indicate the following in a majority of each laminopathic cell population: +, this protein has the same localization and density in/near the nuclear envelope as in wild-type littermates; ++, this protein has the same localization as in wild-type littermates, but with a higher density in the nuclear envelope; −, this protein has largely disappeared from the nuclear envelope; and *, see Fig. S1 in Data S1 for details about lamin A detection. See Fig. 1 for illustrative immunofluorescence micrographs.

Since cell polarization involves the guided reorientation of the MTOC (39), we hypothesized that the weakening of the association between the MTOC and the nucleus would translate to a cell's decreased ability to polarize. MTOC polarization was assessed using a recently described flow-based assay (40), in which cells were subjected to a mild shear stimulus, sufficient to induce polarization but not cell migration (Fig. 3 *A*). Flow-induced polarization of the MTOC was indeed abrogated in $Lmna^{L530P/L530P}$, $Lmna^{-/-}$, and $Emd^{-/y}$ cells, while their wild-type counterparts displayed MTOC polarization in the downstream direction of flow (Fig. 3 *B*). Note that in the absence of flow, the probability of finding the MTOC on either side of the nucleus should be 50%; this was observed in all cells at rest. The effect of shear on nuclear shape was also examined; $Lmna^{L530P/L530P}$ nuclei displayed significant shear defects compared to nonsheared cells, while $Lmna^{-/-}$, $Emd^{-/y}$, and all wild-type nuclei showed no significant shear-dependent effects (Fig. S2 *B* in Data S1).

These results confirm that emerin is required for a tight MTOC-nucleus junction and suggest that it is a key mediator of MTOC positioning with respect to the nucleus and thus, that emerin plays a fundamental role in mediating cell polarization.

Actin structure and deactivation of RhoA in laminopathic cells

Just as the loss of emerin at the NE translated to functional defects dependent on the microtubule network, we hypothesized that disruptions in the LINC complex would similarly disturb the actin architecture of the cell. We investigated whether the cytoplasmic actin filament network, the extent of F-actin bundling, and the morphology of focal adhesions—anchoring sites for actin bundles—were affected in laminopathic cells compared to their wild-type littermates. As was the case with the microtubule network, immunofluorescence microscopy revealed no overt changes in the basal actin cytoskeleton in terms of density and thickness of fibers in mutated cells. Representative results for L530P mutated MAFs, $Lmna^{-/-}$ MEFs, and their wild-type counterparts are shown in Fig. 4 *A* ($Emd^{-/y}$ and respective littermates not

TABLE 2 Summary of the results from functional assays in this study

		Results of functional assays		
Phenotype	Method	MAF $Lmna^{L530P/L530P}$	MEF $Lmna^{-/-}$	MEF $Em^{-/y}$
Focal adhesion density, size, and shape	IF and quantitative image analysis	−	*	−
F-actin architecture and extent of F-actin bundling	IF and spin-down assay	−	−	−
Distance between nucleus and MTOC	IF and quantitative image analysis	**	**	*
Overall shape and shape factor of nucleus	IF and quantitative image analysis	**	**	−
Nucleus deformability	Quantitative image analysis of cells under shear	**	−	−
Cell migration	Wound healing assay	−	*	−
Cell adhesion	Cell-matrix adhesion assay	***	***	−
Cell polarization	Flow-chamber polarization assay	*	*	*
Cell mechanics	Ballistic intracellular nanorheology assay	***	***	−
RhoA activity	G-LISA	*	**	−
Rac activity	G-LISA	−	−	−

Symbols indicate −, no effect for this tested function in these cells compared to wild-type littermates; *, indicate significant difference in this tested function in these cells compared to their wild-type littermates; ***, $p < 0.001$; **, $p < 0.01$; and *, $p < 0.05$.

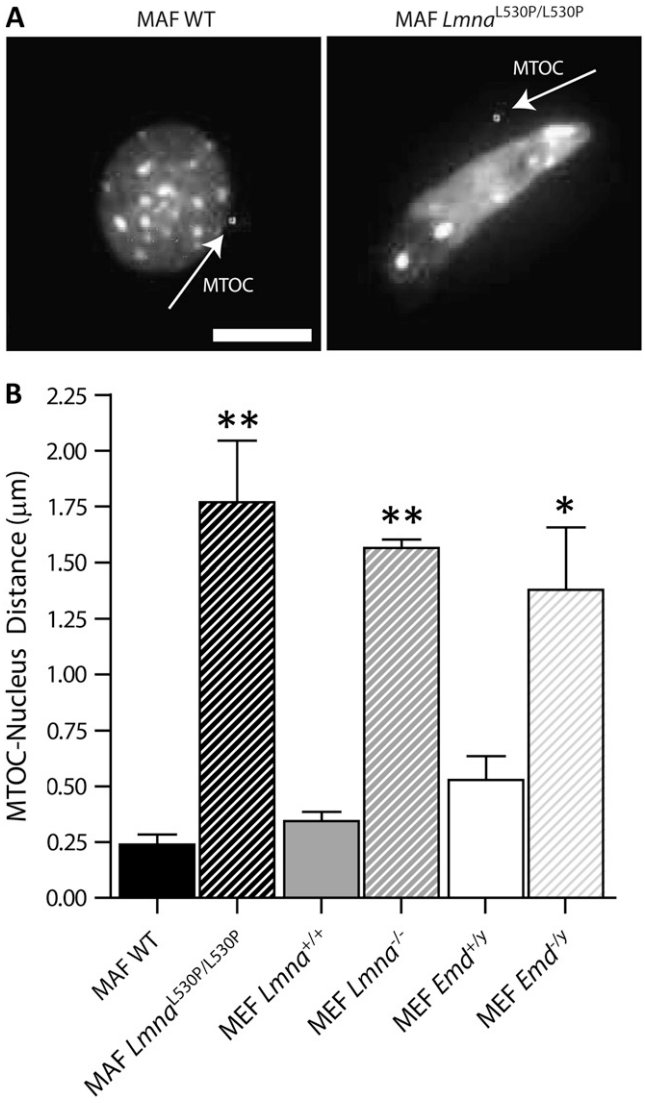

FIGURE 2 Distance between nucleus and MTOC in wild-type and laminopathic fibroblasts. (*A*) Typical distance between nucleus and MTOC in wild-type and $Lmna^{L530P/L530P}$ MAFs. MTOC localization (*open arrows*) was determined by immunofluorescence microscopy using antibodies against γ-tubulin. Nuclear DNA was stained with DAPI. Scale bar, 10 μm. (*B*) Average distance between nucleus and MTOC in wild-type and $Lmna^{L530P/L530P}$, $Lmna^{+/+}$, $Lmna^{-/-}$, $Emd^{+/y}$, and $Emd^{-/y}$ cells. For each type of cell, the nucleus-MTOC distance in at least 20 cells was measured in three independent experiments (total, >60 cells per condition). **, $p < 0.01$; and *, $p < 0.05$. Asterisks shown are relative to corresponding wild-type cells (previous column). In all experiments, cells were plated on collagen.

shown). Further examination of the actin architecture using a spin-down assay revealed no significant differences in the extent of F-actin bundling between laminopathic fibroblasts and their respective wild-type cells (data not shown). Additionally, using quantitative immunofluorescence microscopy (Fig. 4 *A*), we found no significant differences in the area (Fig. 4 *B*), the shape factor (Fig. 4 *C*), and the length (Fig. 4 *D*) of focal adhesions, nor in the number of focal adhesions per cell (Fig. 4 *E*) between $Lmna^{L530P/L530P}$ and wild-type cells. Small but significant differences, however, were detected between $Lmna^{-/-}$ and wild-type fibroblasts; individual focal adhesions in $Lmna^{-/-}$ fibroblasts had a smaller surface area (Fig. 4 *B*), were more rounded as determined by a higher shape factor (Fig. 4 *C*), and were shorter along the longest axis compared to wild-type fibroblasts (Fig. 4 *D*), though no significant difference in the number of focal adhesions per cell was detected between the two lines. We detected no structural actin defects in $Emd^{-/y}$ fibroblasts. Thus, while neither the disease-causing mutation L530P nor emerin depletion caused major reorganization of the actin filament network, small changes were detected at actin-anchoring sites in cells lacking lamin A/C.

Although no drastic changes were observed in actin or focal adhesion architecture of $Lmna^{L530P/L530P}$ fibroblasts relative to wild-type fibroblasts, a small but significant deactivation of the small GTPase RhoA—but not Rac—was detected (Fig. 5, *D* and *E*). The Rho family of small GTPases regulates stress fiber and focal adhesion assembly, while Rac controls peripheral actin in the form of lamellipodia and membrane ruffles (41). Consistent with changes in focal adhesion architecture in $Lmna^{-/-}$ fibroblasts, RhoA activation levels were also significantly lower in these cells, while Rac levels showed no differences compared to the wild-type population (Fig. 5, *D* and *E*). In contrast to the laminopathic models, emerin-null fibroblasts showed no significant changes in activation levels of RhoA and Rac compared to wild-type cells (Fig. 5, *D* and *E*). These results suggest a correlation between decreased RhoA activation and the lack of functional LINC-based nucleus-cytoskeleton connections.

Defects in cell migration and cell adhesion in laminopathic cells

While gross abnormalities in cytoskeletal architecture were not detected in $Lmna^{L530P/L530P}$ and $Lmna^{-/-}$ cells, we tested cell functions that depended directly on these cytoskeletons, including cell migration, cell adhesion, and cell micromechanics. Our previous work (9) has shown that lamin A/C-deficient cells display a slight but significant cell-migration defect in an in vitro wound-healing assay on collagen-coated coverslips (Fig. 5 *B*). Here, using the same wound-healing assay (Fig. 5 *A*), we found that the rate of migration of $Lmna^{L530P/L530P}$ cells did not differ significantly from their wild-type counterparts (Fig. 5 *B*). Similarly, emerin-deficient cells showed no defect in cell migration (Fig. 5 *B*).

To further probe the effect of a defective LINC complex, we investigated the actin-dependent function of cell adhesion. RhoA activation is known to regulate cell adhesion through acto-myosin contractility (42), and we thus hypothesized that a disrupted LINC complex and decreased RhoA activation would correlate with weakened cell adhesion. Using a quantitative cell-matrix adhesion assay in which cells were plated on collagen (see details in Materials and Methods), we found that both $Lmna^{L530P/L530P}$ and $Lmna^{-/-}$

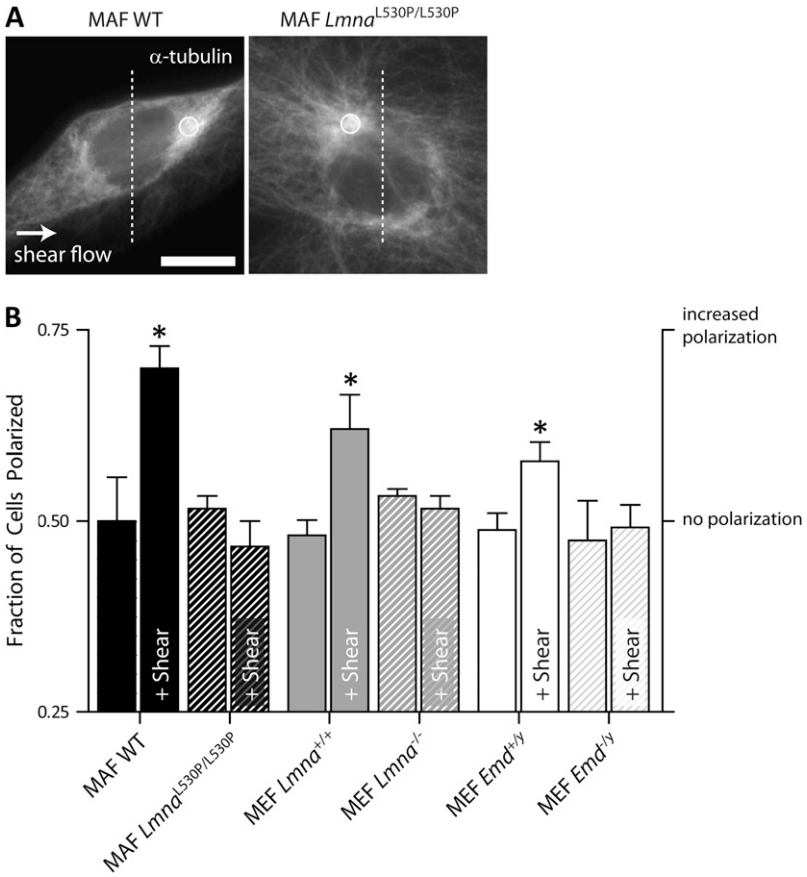

FIGURE 3 Shear-induced polarization is abrogated in laminopathic fibroblasts. (*A*) Typical position of the MTOC with respect to the nucleus in a wild-type (*left panel*) and an $Lmna^{L530P/\ L530P}$ (*right panel*) MAF, both under flow conditions. Cells were subjected to shear flow for 40 min at a wall shear stress of 20 dyn/cm^2, then fixed and stained with DAPI (nuclear DNA) and an antibody against α-tubulin (α-tubulin/Alexa568), and scored for the fraction of cells with MTOCs (*circled*) facing away from the flow direction (i.e., located to the right of a midline through the nucleus). The flow direction is from left to right. In the absence of shear; the probability to find the MTOC at the left of the nucleus is ~50%. Scale bar, 10 μm. (*B*) Average position of the MTOC with respect to the nucleus in both unsheared and sheared wild-type and $Lmna^{L530P/L530P}$ (MAFs), $Lmna^{+/+}$, $Lmna^{-/-}$, $Emd^{+/y}$, and $Emd^{-/y}$ (MEF) cells. For each type of cell and test condition (no shear and shear), the relative position of the MTOC with respect to the nucleus in at least 20 cells was measured in at least three independent experiments (total, >60 cells per condition). *, $p < 0.05$. Asterisks shown are relative to corresponding wild-type cells (previous column). In all experiments, cells were plated on collagen.

fibroblasts had a significantly diminished ability to adhere to substrata compared to their respective wild-type littermates (Fig. 5 *C*). Emerin depletion had no significant effect on cell adhesion (Fig. 5 *C*). Together these results suggest that laminopathic defects such as a defective LINC complex greatly reduce cell-substratum adhesion and that emerin-based linkages between the nucleus and cytoskeleton do not play a significant role in either cell adhesion or cell migration.

Defect in cytoplasmic micromechanics

In concert with the laminopathic structural hypothesis, recent results have suggested that a functional nucleus-cytoskeleton connection is essential to the overall mechanical integrity of the cytoplasm of healthy cells (9). Moreover, cytoplasmic stiffness depends on the level of RhoA activation: elevated levels of RhoA activity are associated with a stiffer cytoplasm (43). Therefore, we hypothesized that $Lmna^{L530P/L530P}$ cells, which show both a significant displacement of major components of the LINC complex and a lowered level of RhoA activation, would have a softer (i.e., less elastic) cytoplasm than their wild-type littermates. To probe the intracellular micromechanics of living cells, 100-nm diameter carboxy-modified polystyrene nanoparticles were introduced directly into the cytoplasm of adherent cells using ballistic injection. The spontaneous displacements of these beads, which were evenly dispersed throughout the cytoplasm (Fig. 6 *A*), were tracked with high spatial and temporal resolution using high-magnification fluorescence microscopy and multiple-particle tracking software (44). We verified that the tracked nanoparticles did not show any directed motion. Indeed, their time-lag-dependent MSDs did not grow faster-than-linearly with time lag (see more in Materials and Methods). The magnitude of the MSDs of the nanoparticles embedded in the cytoplasm of $Lmna^{L530P/L530P}$ cells was significantly higher ($p < 0.001$) than those embedded in wild-type cells over a wide range of timescales (Fig. 6 *B*). Accordingly, the elasticity (i.e., stiffness or stretchiness) of the cytoplasm of $Lmna^{L530P/L530P}$ cells, computed from the nanoparticles' MSDs, was significantly lower than that of wild-type cells (Fig. 6 *C*). The extent of softening of the cytoplasm in $Lmna^{L530P/L530P}$ cells was slightly lower than that caused by lamin A/C depletion compared to their corresponding wild-type counterparts (Fig. 6 *C*): 43% and 69%, respectively. Once again, emerin depletion had no significant effect on the viscoelastic properties of the cytoplasm (Fig. 6 *C*). These results correlate positively with our recent demonstration that disruption of LINC complexes leads to a similar reduction in cytoplasmic elasticity (45). Hence both lamin A/C disease-causing mutation and depletion, but not emerin depletion, produce significant softening of the cytoplasm through weakened nucleo-cytoskeletal connections.

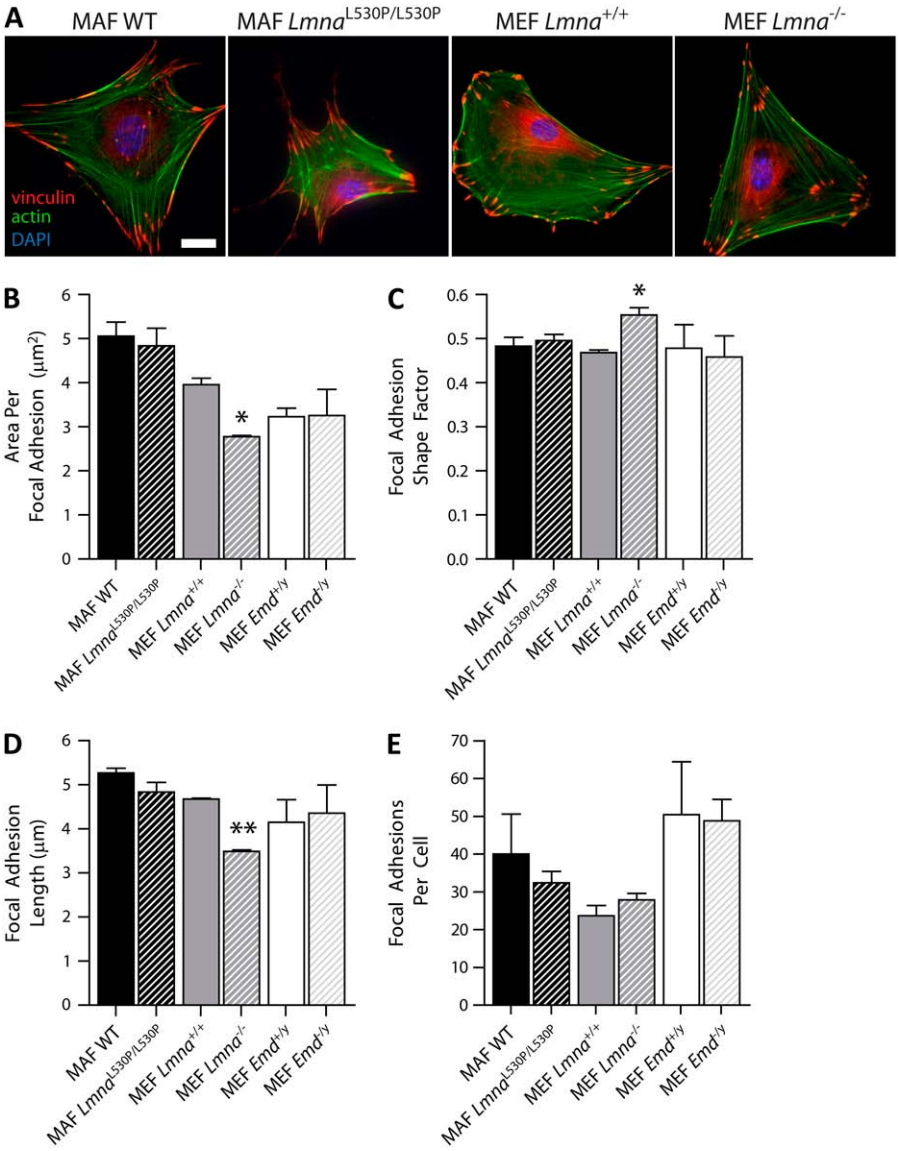

FIGURE 4 Basal actin cytoskeleton architecture. (*A*) Typical actin filament and focal adhesion organization in wild-type and $Lmna^{L530P/\ L530P}$ MAFs and wild-type and $Lmna^{-/-}$ MEFs. Cells were plated on collagen, then fixed and stained for actin (*green*) and focal adhesion protein vinculin (*red*) using phalloidin 488 and anti-vinculin/Alexa-Fluor 568, respectively. Scale bar, 20 μm. (*B*) Average area per focal adhesion, determined by tracing of vinculin-containing focal adhesions followed by morphometric analysis. (*C*) Average focal adhesion shape factor. (*D*) Average length of long axis of focal adhesions. (*E*) Average number of focal adhesions per cell. Focal adhesions were analyzed in at least 10 cells per condition, repeated in three independent experiments (total, >30 cells per condition; ~1000 focal adhesions per condition).

DISCUSSION

Laminopathies, though varied in their manifestation of symptoms, have been commonly linked to mutations in the *Lmna* gene. While the genetic lesions associated to these are well established, the mechanism by which these mutations ultimately cause tissue and muscle defects is less clear. Using fibroblasts of laminopathic models of HGPS and EDMD, two major laminopathies, we investigate functional defects associated with *Lmna* mutations in an effort to elucidate the transition from mutation to disease. Using immunofluorescence microscopy, we demonstrate that nucleo-cytoskeletal connections—namely an emerin-mediated linkage of nucleus and MTOC and an actin/plectin-binding LINC complexes—are disrupted, with LINC complex disruption occurring exclusively in the laminopathic models. Thus, the differential expression of LINC complexes proteins across the three lines studied (intact in $Emd^{-/y}$ cells or disrupted in $Lmna^{L530P/L530P}$ and $Lmna^{-/-}$ cells) allow us to draw conclusions regarding their functions. Fig. 7 summarizes the localization and functions of nuclear membrane proteins in wild-type cells, as well as the demonstrated interactions between inner and outer nuclear membrane proteins that physically tether the nuclear lamina to the cytoskeleton.

New function for the NE protein emerin: control of cell polarization

The present and two recent studies (9,38) have similarly described that cells lacking either lamin A/C or emerin show an interphase centrosome that is detached from the NE compared to their respective wild-type littermates. Here we show that distancing of the MTOC from the NE also occurs in $Lmna^{L530P/L530P}$ cells and to the same or larger extent than in $Lmna^{-/-}$ and $Emd^{-/y}$ cells. Notably, the nucleus-centrosome

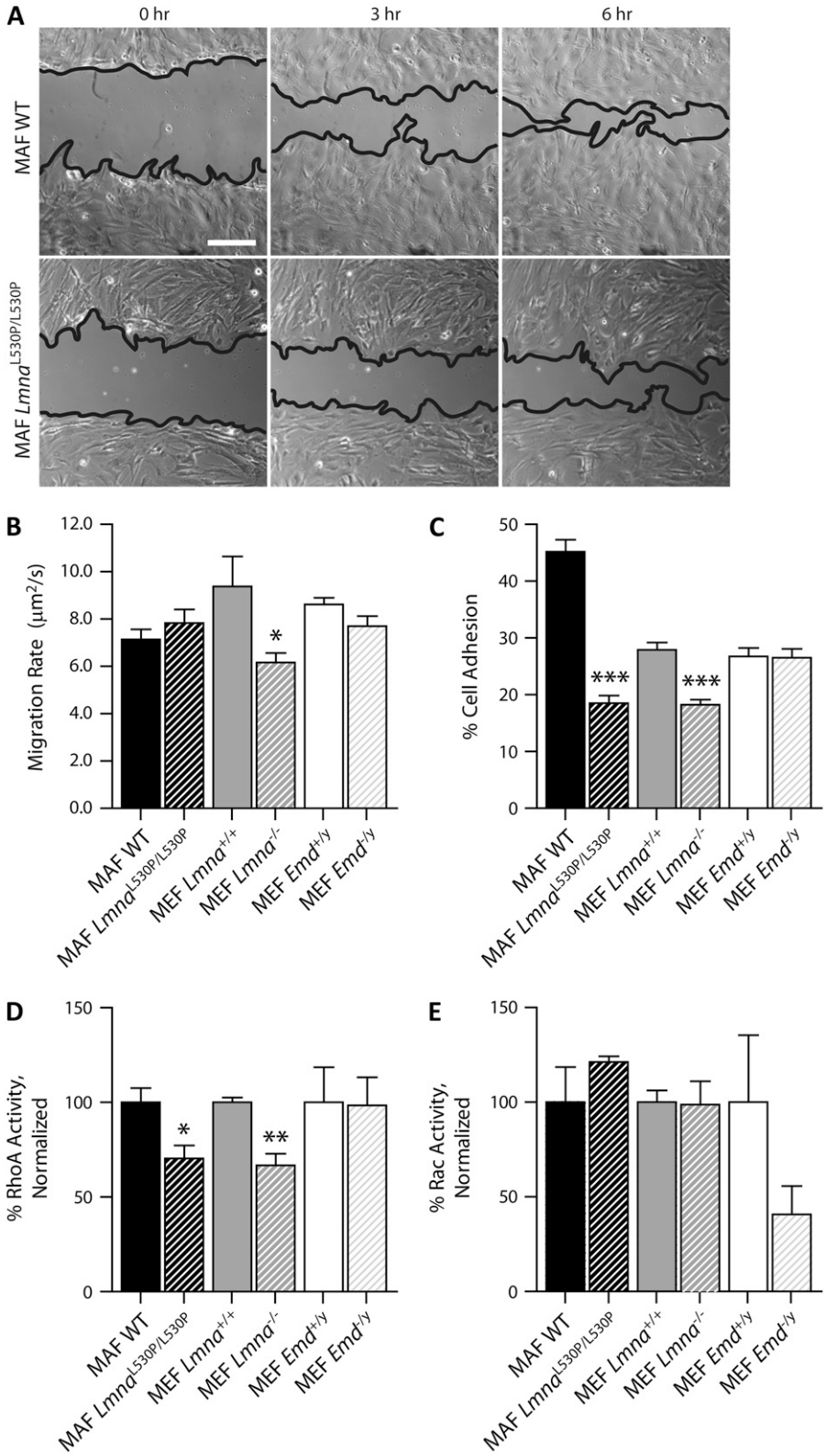

FIGURE 5 Cell migration, cell adhesion, and small GTPase activity in wild-type and laminopathic fibroblasts. (*A*) Typical time-dependent closure of an in vitro wound applied to wild-type (*top panels*) and $Lmna^{L530P/\ L530P}$ (*bottom panels*) MAFs. Wound edges (shown in *black* as guides to the eye) were tracked by time-lapse phase-contrast microscopy over 6 h in an incubated, 5% CO_2 chamber, mounted on a microscope. Scale bar, 200 μm. (*B*) Rate of wound healing in wild-type and $Lmna^{L530P/L530P}$ (MAFs), $Lmna^{+/+}$, $Lmna^{-/-}$, $Emd^{+/y}$, and $Emd^{-/y}$ cells. For each condition, the rate of healing was measured in at least six different wounds whose initial width was within 50 μm of the total average wound size. (*C*) Cell-matrix adhesion as measured by a simple cell adhesion chamber assay (see text for details). The cell adhesion assay was performed using microtiter plates and was repeated in three independent experiments with adhesion measured in at least 36 wells per condition. (*D*) Average, normalized levels of activation in small GTPase RhoA. (*E*) Average, normalized levels of activation in small GTPase Rac. For each condition, the activation assay was performed in three independent experiments. ***, $p < 0.001$; **, $p < 0.01$; and *, $p < 0.05$. Asterisks shown are relative to corresponding wild-type cells (previous column). In all experiments, cells were plated on collagen.

connection in these cells does not appear to be entirely ruptured since centrosomes in these cells are not located in random locations in the cytoplasm, such as the lamella, but rather in the perinuclear region. The absence of emerin seems to be the only major NE protein that is affected in $Emd^{-/y}$ fibroblasts. In $Lmna^{-/-}$ and $Lmna^{L530P/L530P}$ fibroblasts, emerin is also displaced, along with other NE proteins. Together, these results and the MTOC positioning phenotype

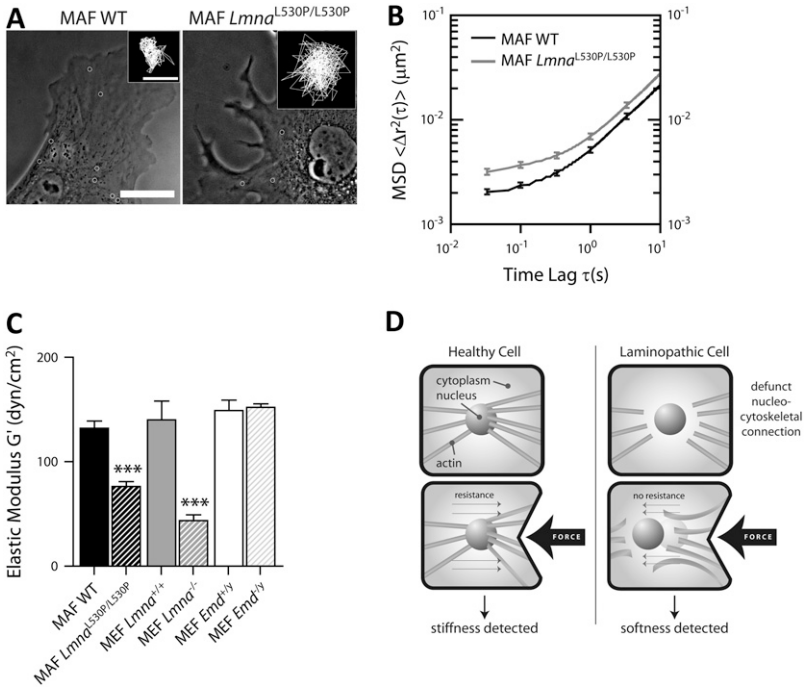

FIGURE 6 Intracellular microrheology of wild-type and laminopathic fibroblasts. (*A*) Fluorescent 100-nm diameter polystyrene nanoparticles were ballistically injected in wild-type (*left panel*) and $Lmna^{L530P/\ L530P}$ (*right panel*) MAFs. Fluorescent micrographs of nanoparticles (outlined in *white circles*) were superimposed on phase-contrast micrographs of cells. Representative trajectories of nanoparticles are also shown at the top right (*inset*) of each micrograph. Micrograph scale bar, 20 μm; inset scale bar, 0.1 μm. (*B*) Nanoparticles were subsequently tracked with high spatial (<10 nm) and temporal (>1/30 s) resolutions using multiparticle tracking software. Ensemble-averaged mean-squared displacements of nanoparticles embedded in the cytoplasm of wild-type (*bottom black curve*) and $Lmna^{L530P/\ L530P}$ (*top gray curve*) MAFs are shown. (*C*) Mean elasticity of the cytoplasm in wild-type and $Lmna^{L530P/L530P}$ cells (MAFs), $Lmna^{+/+}$, $Lmna^{-/-}$, $Emd^{+/y}$, and $Emd^{-/y}$ cells (MEFs). For each condition, the microrheology of at least 10 different cells was measured in three independent experiments (total, >30 cells per condition; >300 nanoparticles per condition). (*D*) Simplified cellular model depicting the intracellular mechanics of healthy and laminopathic cells. Healthy cells in which the nucleo-cytoskeletal connections are intact will resist force of large magnitude, while laminopathic cells cannot resist such forces as well even when actin filament architecture in these cells remains largely intact, due to defunct nucleo-cytoskeletal connections. ***, $p < 0.001$. Asterisks shown are relative to corresponding wild-type cells (previous column). In all experiments, cells were plated on collagen.

shared among the three diseased cell models suggest that emerin plays a central role in the positioning of the MTOC with respect to the NE.

We investigated possible functional consequences of this loosened nucleus-centrosome connection and found that the absence of emerin completely abrogated the ability of cells to polarize their MTOC in the direction of externally applied shear flows. In comparison to the more conventional wound-healing assay (e.g., (9)), the flow-based assay avoids potentially confounding effects of cell proliferation, cell-cell interactions,

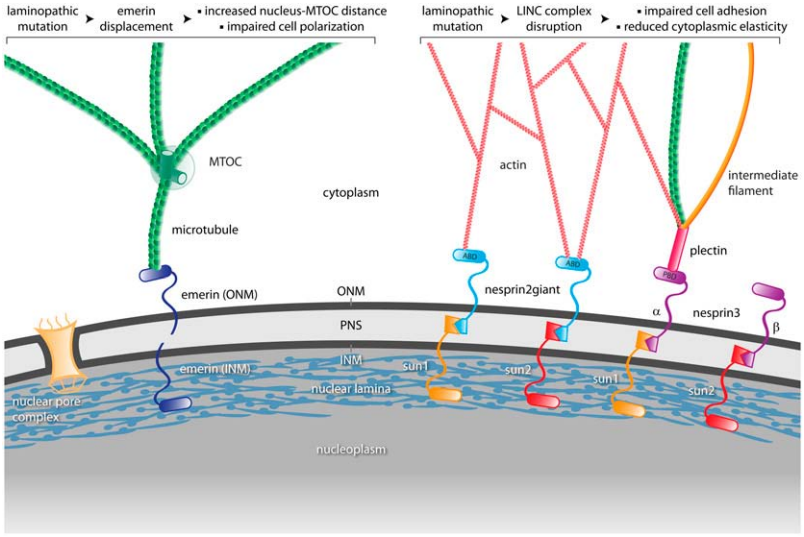

FIGURE 7 Localization of nuclear membrane proteins with respect to the inner and outer nuclear membranes and effects of defunct nucleo-cytoskeletal connections on cell functions. Several proteins interact across the nuclear membrane to form connections between the lamina of the inner nuclear envelope and the cellular cytoskeleton. Interactions in normal cells are shown in the figure, while the functional defects of laminopathic mutations common to both laminopathic models ($Lmna^{L530P/L530P}$ MAF and $Lmna^{-/-}$ MEF) are shown in text above the diagram. Emerin has been shown to localize at the inner nuclear membrane (55) and bind lamin A (15). A recent study also shows that emerin can localize to the outer nuclear membrane and suggests emerin's interaction with microtubules to tether the MTOC to the nucleus (37). Sun proteins localize to the inner nuclear membrane (29,30) and bind nuclear lamins in the nucleoplasmic domain (16,17), while specific Nesprin isoforms, particularly Nesprin2 giant and Nesprin3, localize to the outer nuclear membrane (31,56). Though not represented here, Sun and Nesprin proteins most likely exist as dimers (18,57,58). Sun and Nesprin proteins have been shown to interact promiscuously in the perinuclear space (45). Nesprin2 giant contains an actin-binding domain (ABD) (59), while the α-isoform of Nesprin3 binds plectin (31), a multidomain protein capable of interacting with actin, intermediate filaments, and microtubules (60). Collectively, the Sun and Nesprin proteins form the linker of nucleus and cytoskeleton, or LINC, complex, connecting the nuclear lamina to the cytoskeleton. Thus, emerin and the LINC complexes are believed to bridge connections between lamins of the inner nuclear envelope and the microtubule, actin, and intermediate filament cytoskeletal networks. (*ONM*, outer nuclear membrane; *PNS*, perinuclear space; *INM*, inner nuclear membrane; *ABD*, actin-binding domain; *PBD*, plectin-binding domain; and *MTOC*, microtubule organizing center.)

and net cell migration. We note that the application of flow was mild enough to avoid cell motility, yet sufficient to induce polarization; cell motility was induced at significantly higher shear rates (data not shown). Together these results suggest that a tight connection between the NE and the MTOC is required for the proper polarization of the MTOC in cells under shear or undergoing directed migration into a wound (9) and suggests a new function for emerin in establishing cell polarization.

Laminopathies as cytoskeletal diseases

A distorted nucleus is a morphological hallmark of cells from laminopathic patients or harvested from mouse models of laminopathies (46,47). Our quantitative morphometric analysis shows that $Lmna^{L530P/L530P}$ cells (and to a lesser extent $Lmna^{-/-}$ cells) display ill-shaped nuclei, which are particularly prone to mechanical fragility in cells under shear stresses (Fig. S2 in Data S1). Yet, these cells show defects in functions that do not depend per se on the shape of their nuclei, but depend on their microtubule and actin filament networks, including cell polarization, adhesion, and micromechanics. Moreover, we found that cells lacking lamin A/C and $Lmna^{L530P/L530P}$ cells had significantly reduced levels of RhoA activation compared to their wild-type littermates. As a result of this finding, cells were analyzed in terms of actin stress fiber density and extent of F-actin bundling, yet no significant differences were detected. Thus, while the reduced level of RhoA activity is significant, we hypothesize that the reduction was not sufficient to induce visible changes in actin filament organization through phalloidin staining. Furthermore, even though no significant differences in the architecture of focal adhesions in $Lmna^{L530P/L530P}$ fibroblasts were detected relative to wild-type cells, they had fewer focal adhesions per cell, though the difference was not significant. Nevertheless, this subtle difference, as well as the down-regulation of RhoA activity, could account for the significant decrease in cell adhesion observed in the $Lmna^{L530P/L530P}$ fibroblasts. On the other hand, the focal adhesions of $Lmna^{-/-}$ fibroblasts were morphologically different—significantly smaller, rounder, and shorter—from their respective wild-type cells; such differences, coupled with reduced RhoA activity, most likely contribute to the decrease in cell adhesion observed in the $Lmna^{-/-}$ line.

Together these observations suggest that the phenotypes associated with laminopathies in vivo may not stem directly from defects in nuclear shape or nuclear fragility, but rather from the displacement of key NE proteins due to the lack of, or mutation within, the binding partner lamin, in turn causing major defects in cytoskeleton functions, as revealed here by our biophysical assays.

In laminopathic cells, we observed a drastic displacement of key proteins from the NE, which loosen the physical connections between the lamina and the microtubule (mediated by emerin-MTOC linkage) and actin (mediated by the LINC complex of Sun and Nesprin proteins) and possibly other cytoskeletal networks, which in turn induce major defects in cell functions that depend on these connections. Fig. 7 depicts these physical connections; specifically, emerin can bind microtubules, while Nesprin2 giant can bind actin. Nesprin3 also allows for plectin to link the nucleus to all three cytoskeletal filament systems, including intermediate filaments, F-actin, and microtubules. Our results suggest that a reliable predictive phenotype for the disease state is the softening of the cytoplasm, since cytoskeletal softening was exclusively a feature of cells derived from laminopathic mouse models ($Lmna^{-/-}$ and $Lmna^{L530P/L530P}$), while the mechanical stiffness of $Emd^{-/y}$ cells derived from mice that do not display laminopathic phenotypes was intact. A model schematically depicting these results is shown in Fig. 6 *D*. Healthy cells, in which nucleo-cytoskeletal connections are intact, will resist force-induced deformations, while in laminopathic cells, where such nucleo-cytoskeletal connections are weakened, such deformations will not be resisted, even when actin filament assembly or bundling is unaffected by the mutation. As a result, the cytoplasm of laminopathic cells will appear softer than cells when probed with nanoparticles. It should also be noted that actin stain using phalloidin alone is not an adequate means to assess actin-based changes in cellular stiffness. Indeed, no overt differences in actin stress fibers were detected between wild-type and mutant cells in our studies, whereas ballistic intracellular nanorheology, a much more sensitive and quantitative tool, revealed significant differences in cytoskeletal stiffness. Moreover, physiologically speaking, cellular softening provides a logical rationale for a molecular etiology of laminopathies affecting muscle tissues or skin that are exposed to high mechanical stresses (48). The inability of these cells to withstand such stresses due to cellular softening may lead to functional defects of these tissues.

The fact that cytoplasmic softening is not observed in the $Emd^{-/y}$ model of X-linked EDMD suggests that the lack of cellular polarization, mediated by the loss of emerin from the NE, could be sufficient to spur muscular defects. Cells from both the $Lmna^{-/-}$ AD-EDMD and $Lmna^{L530P/L530P}$ progeric models displayed significantly more defects than the $Emd^{-/y}$ XL-EDMD model, in direct reflection of the severity of these diseases. Though AD-EDMD and XL-EDMD are clinically similar, the X-linked variant due to emerin mutation is less severe; patients affected by AD-EDMD are more likely to suffer from cardiac defects (49). This may explain why the phenotype seen in $Emd^{-/y}$ fibroblasts was significantly milder than that seen in $Lmna^{-/-}$ fibroblasts. This level of correlation between cell-level phenotypes and clinical phenotypes not only reinforces the notion that the mice studied are good models of their respective human diseases, but also further supports the idea that the functional defects elucidated here may explain disease mechanisms at the cellular level.

Despite its central involvement in polarization, our results suggest that emerin plays no significant role in cell functions

that depend critically on the actin filament network, including: controlling actin filament network architecture, the extent of F-actin bundling, focal adhesion morphology, RhoA/Rac1 activation, cell migration, cell adhesion, and intracellular micromechanics. These are somewhat surprising results given the fact that microtubules modulate actin dynamics (50), which regulates cell mechanics (43,51), and regulate focal adhesion assembly (52), which affects cell adhesion (53). Moreover, MTOC polarization typically accompanies directed cell migration (54). Our results, however, indicate that emerin-deficient cells, in which polarization is abrogated, have no defects in cell migration or cell adhesion. Cells in which LINC complexes are disrupted (namely the $Lmna^{L530P/L530P}$ and $Lmna^{-/-}$ lines), however, specifically displayed marked defects in actin-related functions. In particular, loss of elasticity in these laminopathic fibroblasts agrees well with recent results in which the disruption of endogenous LINC complexes has marked effects on cytoplasmic stiffness (45). Possible defects to the intermediate filament network caused by laminopathic mutations, though not explored in detail here, should also be considered as potential mechanisms by which defunct LINC connections manifest as disease. Together our studies establish two functionally and biochemically distinct pathways that connect the lamina to the cytoskeleton: 1), emerin, which binds microtubules and mediates centrosome position near the nucleus and centrosome polarization during migration or stimulation by shear flows; and 2), the LINC complexes, which connect the lamina to the actin network and mediates cell adhesion (though not through changes in focal adhesion morphology), cell migration (though not through a defect in cell polarization), and cytoplasmic micromechanics.

SUPPLEMENTARY MATERIAL

To view all of the supplemental files associated with this article, visit www.biophysj.org.

This work was partly supported by National Institutes of Health No. grant GM084204 (to D.W. and D.H.) and a Muscular Dystrophy Association grant (to D.H.).

REFERENCES

1. Capell, B. C., and F. S. Collins. 2006. Human laminopathies: nuclei gone genetically awry. *Nat. Rev. Genet.* 7:940–952.
2. Eriksson, M., W. T. Brown, L. B. Gordon, M. W. Glynn, J. Singer, L. Scott, M. R. Erdos, C. M. Robbins, T. Y. Moses, P. Berglund, A. Dutra, E. Pak, S. Durkin, A. B. Csoka, M. Boehnke, T. W. Glover, and F. S. Collins. 2003. Recurrent de novo point mutations in lamin A cause Hutchinson-Gilford progeria syndrome. *Nature.* 423:293–298.
3. Chen, L., L. Lee, B. A. Kudlow, H. G. Dos Santos, O. Sletvold, Y. Shafeghati, E. G. Botha, A. Garg, N. B. Hanson, G. M. Martin, I. S. Mian, B. K. Kennedy, and J. Oshima. 2003. LMNA mutations in atypical Werner's syndrome. *Lancet.* 362:440–445.
4. Manilal, S., T. M. Nguyen, C. A. Sewry, and G. E. Morris. 1996. The Emery-Dreifuss muscular dystrophy protein, emerin, is a nuclear membrane protein. *Hum. Mol. Genet.* 5:801–808.
5. Charniot, J. C., C. Pascal, C. Bouchier, P. Sebillon, J. Salama, L. Duboscq-Bidot, M. Peuchmaurd, M. Desnos, J. Y. Artigou, and M. Komajda. 2003. Functional consequences of an LMNA mutation associated with a new cardiac and non-cardiac phenotype. *Hum. Mutat.* 21:473–481.
6. Wilson, K. L., M. S. Zastrow, and K. K. Lee. 2001. Lamins and disease: insights into nuclear infrastructure. *Cell.* 104:647–650.
7. Gruenbaum, Y., A. Margalit, R. D. Goldman, D. K. Shumaker, and K. L. Wilson. 2005. The nuclear lamina comes of age. *Nat. Rev. Mol. Cell Biol.* 6:21–31.
8. Holaska, J. M., K. L. Wilson, and M. Mansharamani. 2002. The nuclear envelope, lamins and nuclear assembly. *Curr. Opin. Cell Biol.* 14:357–364.
9. Lee, J. S., C. M. Hale, P. Panorchan, S. B. Khatau, J. P. George, Y. Tseng, C. L. Stewart, D. Hodzic, and D. Wirtz. 2007. Nuclear lamin A/C deficiency induces defects in cell mechanics, polarization, and migration. *Biophys. J.* 93:2542–2552.
10. Stewart, C. L., K. J. Roux, and B. Burke. 2007. Blurring the boundary: the nuclear envelope extends its reach. *Science.* 318:1408–1412.
11. Vergnes, L., M. Peterfy, M. O. Bergo, S. G. Young, and K. Reue. 2004. Lamin B1 is required for mouse development and nuclear integrity. *Proc. Natl. Acad. Sci. USA.* 101:10428–10433.
12. Gerace, L., and G. Blobel. 1980. The nuclear envelope lamina is reversibly depolymerized during mitosis. *Cell.* 19:277–287.
13. Stewart, C., and B. Burke. 1987. Teratocarcinoma stem cells and early mouse embryos contain only a single major lamin polypeptide closely resembling lamin B. *Cell.* 51:383–392.
14. Rober, R. A., K. Weber, and M. Osborn. 1989. Differential timing of nuclear lamin A/C expression in the various organs of the mouse embryo and the young animal: a developmental study. *Development.* 105:365–378.
15. Clements, L., S. Manilal, D. R. Love, and G. E. Morris. 2000. Direct interaction between emerin and lamin A. *Biochem. Biophys. Res. Commun.* 267:709–714.
16. Crisp, M., Q. Liu, K. Roux, J. B. Rattner, C. Shanahan, B. Burke, P. D. Stahl, and D. Hodzic. 2006. Coupling of the nucleus and cytoplasm: role of the LINC complex. *J. Cell Biol.* 172:41–53.
17. Worman, H. J., and G. G. Gundersen. 2006. Here come the SUNs: a nucleocytoskeletal missing link. *Trends Cell Biol.* 16:67–69.
18. Ketema, M., K. Wilhelmsen, I. Kuikman, H. Janssen, D. Hodzic, and A. Sonnenberg. 2007. Requirements for the localization of nesprin-3 at the nuclear envelope and its interaction with plectin. *J. Cell Sci.* 120: 3384–3394.
19. Zhang, Q., C. Bethmann, N. F. Worth, J. D. Davies, C. Wasner, A. Feuer, C. D. Ragnauth, Q. Yi, J. A. Mellad, D. T. Warren, M. A. Wheeler, J. A. Ellis, J. N. Skepper, M. Vorgerd, B. Schlotter-Weigel, P. L. Weissberg, R. G. Roberts, M. Wehnert, and C. M. Shanahan. 2007. Nesprin-1 and -2 are involved in the pathogenesis of Emery Dreifuss muscular dystrophy and are critical for nuclear envelope integrity. *Hum. Mol. Genet.* 16:2816–2833.
20. Markiewicz, E., T. Dechat, R. Foisner, R. A. Quinlan, and C. J. Hutchison. 2002. Lamin A/C binding protein LAP2α is required for nuclear anchorage of retinoblastoma protein. *Mol. Biol. Cell.* 13:4401–4413.
21. Vlcek, S., T. Dechat, and R. Foisner. 2001. Nuclear envelope and nuclear matrix: interactions and dynamics. *Cell. Mol. Life Sci.* 58: 1758–1765.
22. Broers, J. L., E. A. Peeters, H. J. Kuijpers, J. Endert, C. V. Bouten, C. W. Oomens, F. P. Baaijens, and F. C. Ramaekers. 2004. Decreased mechanical stiffness in $LMNA^{-/-}$ cells is caused by defective nucleocytoskeletal integrity: implications for the development of laminopathies. *Hum. Mol. Genet.* 13:2567–2580.
23. Lammerding, J., P. C. Schulze, T. Takahashi, S. Kozlov, T. Sullivan, R. D. Kamm, C. L. Stewart, and R. T. Lee. 2004. Lamin A/C deficiency causes defective nuclear mechanics and mechanotransduction. *J. Clin. Invest.* 113:370–378.

24. Mounkes, L. C., S. Kozlov, L. Hernandez, T. Sullivan, and C. L. Stewart. 2003. A progeroid syndrome in mice is caused by defects in A-type lamins. *Nature*. 423:298–301.
25. Sullivan, T., D. Escalante-Alcalde, H. Bhatt, M. Anver, N. Bhat, K. Nagashima, C. L. Stewart, and B. Burke. 1999. Loss of A-type lamin expression compromises nuclear envelope integrity leading to muscular dystrophy. *J. Cell Biol.* 147:913–920.
26. Bione, S., E. Maestrini, S. Rivella, M. Mancini, S. Regis, G. Romeo, and D. Toniolo. 1994. Identification of a novel X-linked gene responsible for Emery-Dreifuss muscular dystrophy. *Nat. Genet.* 8:323–327.
27. Lammerding, J., J. Hsiao, P. C. Schulze, S. Kozlov, C. L. Stewart, and R. T. Lee. 2005. Abnormal nuclear shape and impaired mechanotransduction in emerin-deficient cells. *J. Cell Biol.* 170:781–791.
28. Melcon, G., S. Kozlov, D. A. Cutler, T. Sullivan, L. Hernandez, P. Zhao, S. Mitchell, G. Nader, M. Bakay, J. N. Rottman, E. P. Hoffman, and C. L. Stewart. 2006. Loss of emerin at the nuclear envelope disrupts the Rb1/E2F and MyoD pathways during muscle regeneration. *Hum. Mol. Genet.* 15:637–651.
29. Haque, F., D. J. Lloyd, D. T. Smallwood, C. L. Dent, C. M. Shanahan, A. M. Fry, R. C. Trembath, and S. Shackleton. 2006. SUN1 interacts with nuclear lamin A and cytoplasmic nesprins to provide a physical connection between the nuclear lamina and the cytoskeleton. *Mol. Cell. Biol.* 26:3738–3751.
30. Hodzic, D. M., D. B. Yeater, L. Bengtsson, H. Otto, and P. D. Stahl. 2004. Sun2 is a novel mammalian inner nuclear membrane protein. *J. Biol. Chem.* 279:25805–25812.
31. Wilhelmsen, K., S. H. Litjens, I. Kuikman, N. Tshimbalanga, H. Janssen, I. van den Bout, K. Raymond, and A. Sonnenberg. 2005. Nesprin-3, a novel outer nuclear membrane protein, associates with the cytoskeletal linker protein plectin. *J. Cell Biol.* 171:799–810.
32. Kole, T. P., Y. Tseng, and D. Wirtz. 2004. Intracellular microrheology as a tool for the measurement of the local mechanical properties of live cells. *Methods Cell Biol.* 78:45–64.
33. Lee, J. S., P. Panorchan, C. M. Hale, S. B. Khatau, T. P. Kole, Y. Tseng, and D. Wirtz. 2006. Ballistic intracellular nanorheology reveals ROCK-hard cytoplasmic stiffening response to fluid flow. *J. Cell Sci.* 119:1760–1768.
34. Panorchan, P., J. S. Lee, T. P. Kole, Y. Tseng, and D. Wirtz. 2006. Microrheology and ROCK signaling of human endothelial cells embedded in a 3D matrix. *Biophys. J.* 91:3499–3507.
35. Panorchan, P., J. S. Lee, B. R. Daniels, T. P. Kole, Y. Tseng, and D. Wirtz. 2007. Probing cellular mechanical responses to stimuli using ballistic intracellular nanorheology. *Methods Cell Biol.* 83:115–140.
36. Mason, T. G., K. Ganesan, J. V. van Zanten, D. Wirtz, and S. C. Kuo. 1997. Particle-tracking microrheology of complex fluids. *Phys. Rev. Lett.* 79:3282–3285.
37. Salpingidou, G., A. Smertenko, I. Hausmanowa-Petrucewicz, P. J. Hussey, and C. J. Hutchison. 2007. A novel role for the nuclear membrane protein emerin in association of the centrosome to the outer nuclear membrane. *J. Cell Biol.* 178:897–904.
38. Tzima, E., M. A. Del Pozo, W. B. Kiosses, S. A. Mohamed, S. Li, S. Chien, and M. A. Schwartz. 2002. Activation of Rac1 by shear stress in endothelial cells mediates both cytoskeletal reorganization and effects on gene expression. *EMBO J.* 21:6791–6800.
39. Lee, J. S., M. I. Chang, Y. Tseng, and D. Wirtz. 2005. Cdc42 mediates nucleus movement and MTOC polarization in Swiss 3T3 fibroblasts under mechanical shear stress. *Mol. Biol. Cell.* 16:871–880.
40. Nobes, C. D., and A. Hall. 1995. Rho, Rac, and Cdc42 GTPases regulate the assembly of multimolecular focal complexes associated with actin stress fibers, lamellipodia, and filopodia. *Cell.* 81:53–62.
41. Etienne-Manneville, S., and A. Hall. 2002. Rho GTPases in cell biology. *Nature.* 420:629–635.
42. Kole, T. P., Y. Tseng, L. Huang, J. L. Katz, and D. Wirtz. 2004. Rho kinase regulates the intracellular micromechanical response of adherent cells to ρ-activation. *Mol. Biol. Cell.* 15:3475–3484.
43. Tseng, Y., T. P. Kole, and D. Wirtz. 2002. Micromechanical mapping of live cells by multiple-particle-tracking microrheology. *Biophys. J.* 83:3162–3176.
44. Stewart-Hutchinson, P. J., C. M. Hale, D. Wirtz, and D. Hodzic. 2008. Structural requirements for the assembly of LINC complexes and their function in cellular mechanical stiffness. *Exp. Cell Res.* 314:1892–1905.
45. Muchir, A., J. Medioni, M. Laluc, C. Massart, T. Arimura, A. J. van der Kooi, I. Desguerre, M. Mayer, X. Ferrer, S. Briault, M. Hirano, H. J. Worman, A. Mallet, M. Wehnert, K. Schwartz, and G. Bonne. 2004. Nuclear envelope alterations in fibroblasts from patients with muscular dystrophy, cardiomyopathy, and partial lipodystrophy carrying lamin A/C gene mutations. *Muscle Nerve.* 30:444–450.
46. Mounkes, L., S. Kozlov, B. Burke, and C. L. Stewart. 2003. The laminopathies: nuclear structure meets disease. *Curr. Opin. Genet. Dev.* 13:223–230.
47. Stehbens, W. E., B. Delahunt, T. Shozawa, and E. Gilbert-Barness. 2001. Smooth muscle cell depletion and collagen types in progeric arteries. *Cardiovasc. Pathol.* 10:133–136.
48. Muntoni, F., G. Bonne, L. G. Goldfarb, E. Mercuri, R. J. Piercy, M. Burke, R. B. Yaou, P. Richard, D. Recan, A. Shatunov, C. A. Sewry, and S. C. Brown. 2006. Disease severity in dominant Emery Dreifuss is increased by mutations in both emerin and desmin proteins. *Brain.* 129:1260–1268.
49. Small, J. V., B. Geiger, I. Kaverina, and A. Bershadsky. 2002. How do microtubules guide migrating cells? *Nat. Rev. Mol. Cell Biol.* 3:957–964.
50. Kole, T. P., Y. Tseng, I. Jiang, J. L. Katz, and D. Wirtz. 2005. Intracellular mechanics of migrating fibroblasts. *Mol. Biol. Cell.* 16:328–338.
51. Krylyshkina, O., K. I. Anderson, I. Kaverina, I. Upmann, D. J. Manstein, J. V. Small, and D. K. Toomre. 2003. Nanometer targeting of microtubules to focal adhesions. *J. Cell Biol.* 161:853–859.
52. Lauffenburger, D. A., and A. F. Horwitz. 1996. Cell migration: a physically integrated molecular process. *Cell.* 84:359–369.
53. Gomes, E. R., S. Jani, and G. G. Gundersen. 2005. Nuclear movement regulated by Cdc42, MRCK, myosin, and actin flow establishes MTOC polarization in migrating cells. *Cell.* 121:451–463.
54. Gerace, L., A. Blum, and G. Blobel. 1978. Immunocytochemical localization of the major polypeptides of the nuclear pore complex-lamina fraction. Interphase and mitotic distribution. *J. Cell Biol.* 79:546–566.
55. Manilal, S., T. M. Nguyen, and G. E. Morris. 1998. Colocalization of emerin and lamins in interphase nuclei and changes during mitosis. *Biochem. Biophys. Res. Commun.* 249:643–647.
56. Zhang, Q., J. N. Skepper, F. Yang, J. D. Davies, L. Hegyi, R. G. Roberts, P. L. Weissberg, J. A. Ellis, and C. M. Shanahan. 2001. Nesprins: a novel family of spectrin-repeat-containing proteins that localize to the nuclear membrane in multiple tissues. *J. Cell Sci.* 114:4485–4498.
57. Crisp, M., and B. Burke. 2008. The nuclear envelope as an integrator of nuclear and cytoplasmic architecture. *FEBS Lett.* 582:2023–2032.
58. Wang, Q., X. Du, Z. Cai, and M. I. Greene. 2006. Characterization of the structures involved in localization of the SUN proteins to the nuclear envelope and the centrosome. *DNA Cell Biol.* 25:554–562.
59. Zhen, Y. Y., T. Libotte, M. Munck, A. A. Noegel, and E. Korenbaum. 2002. NUANCE, a giant protein connecting the nucleus and actin cytoskeleton. *J. Cell Sci.* 115:3207–3222.
60. Svitkina, T. M., A. B. Verkhovsky, and G. G. Borisy. 1996. Plectin sidearms mediate interaction of intermediate filaments with microtubules and other components of the cytoskeleton. *J. Cell Biol.* 135:991–1007.